

Article

# An Integrated Analytical Approach to Define the Compositional and Textural Features of Mortars Used in the Underwater Archaeological Site of Castrum Novum (Santa Marinella, Rome, Italy)

Luciana Randazzo <sup>1</sup>, Michela Ricca <sup>1</sup>, Silvestro Ruffolo <sup>1</sup>, Marco Aquino <sup>2</sup>, Barbara Davide Petriaggi <sup>3</sup>, Flavio Enei <sup>4</sup> and Mauro F. La Russa <sup>1,5,\*</sup>

<sup>1</sup> Department of Biology, Ecology and Earth Sciences (DiBEST), University of Calabria, 87036 Arcavacata di Rende, Cosenza, Italy; luciana.randazzo@unical.it (L.R.); michela.ricca@unical.it (M.R.); silvio.ruffolo79@gmail.com (S.R.)

<sup>2</sup> Department of Environmental and Chemical Engineering (DIATIC), University of Calabria, 87036 Arcavacata di Rende, Cosenza, Italy; marco.aquino1992@libero.it

<sup>3</sup> Ministero dei Beni e delle Attività Culturali e del Turismo—Istituto Superiore per la Conservazione e il Restauro, 00153 Rome, Italy; barbara.davide@beniculturali.it

<sup>4</sup> Museo del Mare e della Navigazione Antica, Castello di Santa Severa, 00058 S. Severa, Rome, Italy; fenei@comune.santamarinella.rm.it

<sup>5</sup> Institute of Atmospheric Sciences and Climate, National Research Council, Via Gobetti 101, 40129 Bologna, Italy

\* Correspondence: mauro.larussa@unical.it

Received: 19 March 2019; Accepted: 29 April 2019; Published: 30 April 2019



**Abstract:** This paper aims to carry out an archaeometric characterization of mortar samples taken from an underwater environment. The fishpond of the archaeological site of Castrum Novum (Santa Marinella, Rome, Italy) was chosen as a pilot site for experimentation. The masonry structures reached the maximum thickness at the apex of the fishpond (4.70 m) and consisted of a concrete conglomerate composed of slightly rough stones of medium size bound with non-hydraulic mortar. After sampling, for a complete characterization of selected mortar fragments, different and complementary techniques (stereomicroscopy, polarizing optical microscopy, and X-ray powder diffraction analysis) were carried out in order to: a) define the minero-petrographic features; and b) investigate their state of conservation. The obtained data allowed the determination of the main constituents of mortars from a compositional point of view. The raw materials, in fact, were quite homogeneous, as well as the ratio in which they were mixed, confirming the typical "recipe" used in Roman times to manufacture hydraulic-type mortars by adding pozzolana. At the same time, it was possible to identify the various degradation processes we were interested in, namely, biological colonization (bio-fouling) that develops differently according to environmental conditions. Based on characterization phase results, the research will help to develop adequate techniques for intervention (innovative tools and methods for the protection of underwater cultural heritage) with particular regard to cleaning and consolidating procedures to be carried out directly in situ.

**Keywords:** pozzolana; hydraulic-type mortars; minero-petrographic analysis; restoration

## 1. Introduction

In recent decades, interest in the study of degradation phenomena affecting archaeological sites located in submarine environments has increased significantly. Furthermore, innovative approaches for their protection have been developed [1–9]. The most recent guidelines of scientific and international

cultural heritage protection organisms strive to foster the promotion, protection, and in situ preservation of underwater archaeological and historical heritage (UNESCO Convention on the Protection of the Underwater Cultural Heritage, 2 November 2001). One of the main causes of the decay of stone materials in an underwater environment is biodeterioration [3–6] in the form of biofouling and bioerosion phenomena [10].

This study is part of the MaTACoS Project (Materiali e Tecnologie avanzate applicate alla conservazione subacquea—Advanced materials and techniques for underwater conservation), funded by the Italian Ministry of Economic Development (MISE). The project focuses on the development of innovative tools and methods for the protection of underwater cultural heritage, with particular regard to cleaning and consolidating procedures to be carry out directly in situ.

The aim of the project is, in fact, the study and characterization of archaeological materials and their degradation forms in the pilot site and the experimentation with innovative mortars, to be applied directly in situ, in order to limit the biological growth. The fishpond located at the archaeological site of Castrum Novum was chosen as a pilot site for the experimentation.

Castrum Novum was a Roman colony whose ruins are located between Torre Chiaruccia and Casale Alibrandi. The archaeological site lies on a wide area facing the sea, at the 64.4 km mark of the Aurelia State Road, in the Province of Rome, in a territory corresponding to today's Santa Marinella, which, during the Roman ages, belonged to Caere, now Cerveteri [11,12]. During the first half of the third century BC, it was one of the most important cities found along the ancient Etruscan coast, along with Alsium (now Palo Laziale) and Pyrgi (Santa Severa). Other significant remains, concerning the ancient city and the ancient harbor, lie close to the beach where now some modern stilts stand. The apsidal fishpond, for example, is one of these structures on the coastline. It is composed of only one tank, with an average immersion of 0.37 m below the sea level. It has an NE/SW orientation with a length of 43 m, a width of 25 m, and a surface of about 1100 m<sup>2</sup> (Figure 1).

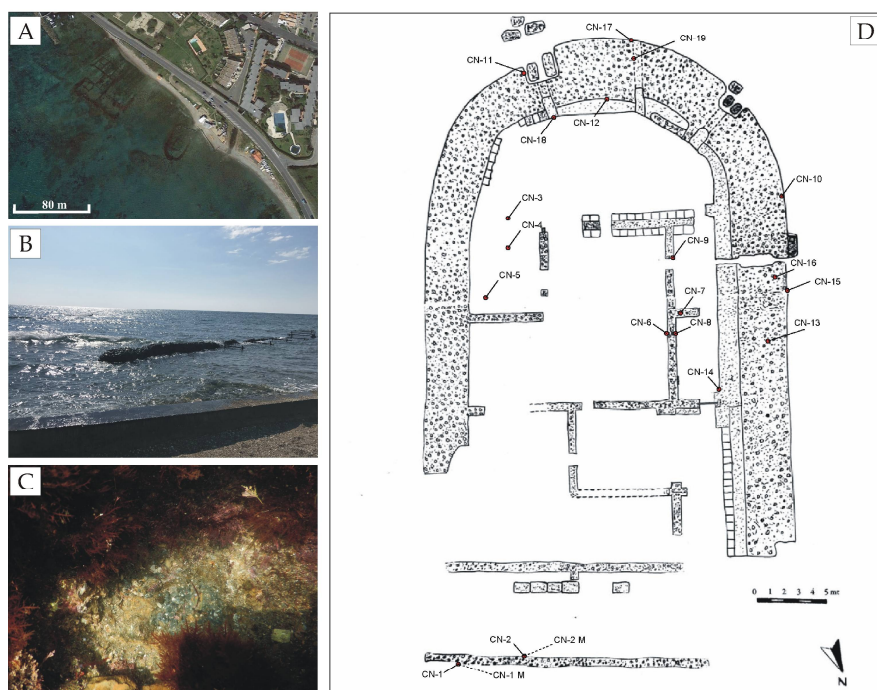


**Figure 1.** (A) Location of Castrum Novum archaeological site; (B) photo of the fishpond partially outcropping above sea level; (C) underwater photo of the fishpond; (D) sketch of the apsidal fishpond composed of only one tank.

The masonry structures reach the maximum thickness at the apex of the fishpond (4.70 m) and the minimum on the south eastern side (3.20 m) and consist of a concrete conglomerate composed of

slightly rough stones of medium size bound with non-hydraulic mortar, while the ground side consists of a concrete wall of which remains a part of 19.0 m in length, 0.60 m in width, and 0.90 m in height [12].

The entire structure rests on an artificial foundation of boulders as is evident from the rapid increase in depth on the NW side and from aerial photography. The structure is divided into three distinct parts: (a) the apsidal part, (b) the central part with walls that delimit at least 10 tanks, and (c) the part on the shore where two parallel walls of different sizes probably delimit a space on the ground, evident from the presence of some stone paving slabs still in situ. The first one, as mentioned, is bounded by a wide pier up to 4.70 m, which has three adduction channels with different inclinations to favor the entry of water. In the apsidal area there are no dividing walls, so it can be deduced that there is a single tank probably used as an enclosure that is a tank for the storage and selection of the fish or the attraction of the fish through introduction of fresh water certainly coming from the adjacent Fosso delle Guardiole.

The first phase of this study, therefore, consisted of the sampling of representative mortar fragments from the fishpond. Samples were then characterized in terms of mineralogical and chemical composition with the aim to verify the ancient recipe used in Roman times and their degradation state. The acquired data should be useful for designing products compatible with the archaeological material for their conservation against biofouling, which is the most aggressive degrading agent in underwater environments.

## 2. Materials and Methods

Seventeen samples were collected directly on site for petrographic, mineralogical, and microchemical investigations (Table 1, Figure 2). All the samples were taken from submerged areas under ~1.5 m of seawater. Immediately after seawater sampling, samples were left in the seawater medium until reaching the laboratories. A washing procedure, through freshwater bath firstly and distilled water secondly, was then performed. The washing procedure was repeated consecutively until the conductivity safe level of 150  $\mu\text{S}$  was reached [13,14]. Finally, the fragments were left to air dry.

Stereomicroscope observations using an EMZ-5D, MEIJI EM were performed in order to preliminarily identify the biological communities and possible decay phenomena occurring in samples during the period of permanence in seawater.

Thin-section petrography was carried out on all samples by means of a Zeiss Axiolab microscope (Zeiss, Oberkochen, Germany) equipped with digital camera. Thin sections (thickness 0.03 mm) were obtained after preliminary under vacuum consolidation by epoxy resin. Both textural and mineralogical features were observed (i.e., percentage ratio between aggregate/binder, grain size, and distribution of the aggregate, presence or absence of binder lumps). The estimation of textural features was made by using comparative charts after [15].

X-ray Powder Diffraction (XRPD) analysis was primarily aimed to identify the mineralogical phases that compose the binder. In order to obtain an enriched specimen of the binder, each sample was manually disaggregated with a wooden pestle and the coarser aggregate grains were picked up under the reflected light stereomicroscope. Successively, the disaggregated specimens were size-sieved and only the finest fraction passing the 0.063 mm sieve was collected because it was considered satisfactorily representative of the binder. XRPD measurements were obtained by a D8 Advance Bruker X-ray diffractometer with Cu K $\alpha$  radiation as the X-ray source. The diffractograms were recorded in the  $2\theta$  range of 0–60°. Measuring conditions were set at 40 kV voltage, 30 mA current, 0.02°  $2\theta$  step size, and 3.0 sec step time.

Finally, electron probe microanalyses coupled with energy-dispersive spectrometry (EPMA-EDS) were carried out by a JEOL JXA 8230 equipment coupled with a JEOL EX-94310FaL1Q silicon drift type EDS. Measurements were conducted on selected glass shards of pumices and volcanic fragments composing the aggregates of mortar samples, as well as on the binder lumps, with the aim to identify, respectively, the volcanic products employed in the mortars and the hydraulic or aerial nature of the binder. The measurements were performed on polished thin sections coated with a thin and

highly conductive graphite film. Furthermore, the acquired data were used to evaluate the hydraulic properties of the binder and of the lime lumps determining the hydraulicity index (HI), according to [16]:  $HI = (SiO_2 + Al_2O_3 + Fe_2O_3)/(CaO + MgO)$ .

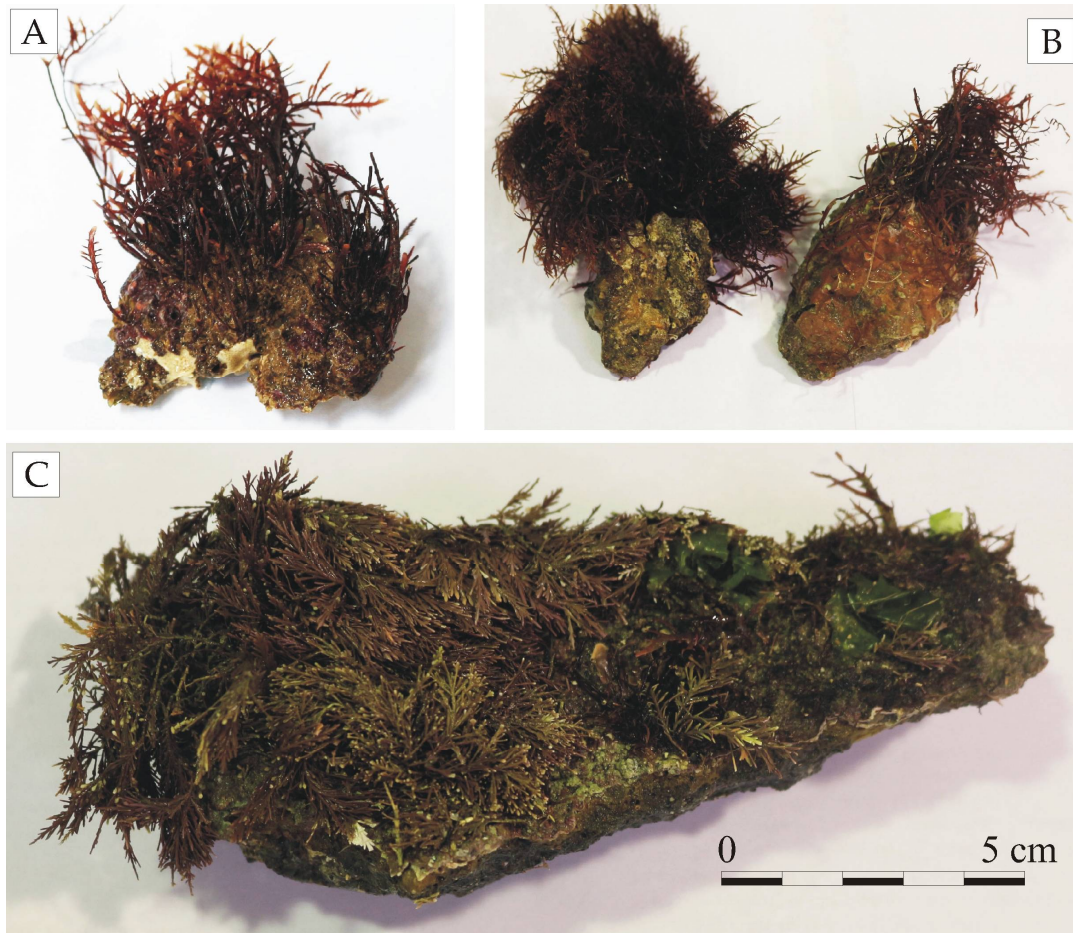


**Figure 2.** Some representative fragments of mortar from underwater archaeological site: (A) macroscopic aspect of the sample CN-2; (B) macroscopic aspect of the sample CN-7; (C) macroscopic aspect of the sample CN-13.

### 3. Results and Discussion

#### 3.1. Stereomicroscopy Observation

Observations of sample surfaces through stereomicroscope revealed some variability in the type of bio-colonization. The rates of coverage due to biological growth were mainly due to encrusting organisms consisting of barnacles, Serpulidae, bryozoans, mollusks, and algae. All collected data are summarized in Table 1.

**Table 1.** Samples and description of alteration level.

Sample Code		Description of Superficial Alteration Level	Typology
1	CN-1	Coherent and compact deposit, mainly whitish in color, alternating with greenish layers. Recognized organisms: barnacles, green and brown algae. Variable thickness ~ 1–3 mm.	coarse aggregate fragment + mortar
2	CN-1M	Brown–greenish layer, mainly due to algal activity and sediment accumulation. Variable thickness ~ 1–3 mm.	mortar
3	CN-2	Brown–greenish layer, mainly due to algal activity and sediment accumulation. Recognized organisms: barnacles and tube-building annelid worms (Serpulidae). Variable thickness ~ 1–5 mm.	mortar
4	CN-2M	Brown–greenish layer, mainly due to algal activity. Variable thickness ~ 1–2 mm.	mortar
5	CN-4	A coherent layer of whitish deposits, mainly due to benthic communities where barnacles and Serpulidae worms prevail. Variable thickness ~ 1–2 mm.	mortar
6	CN-7	Thin layer of compact and coherent whitish deposit, alternating with reddish areas. Presence of encrusting algae in addition to brown algae. Variable thickness ~ 1–5 mm.	mortar
7	CN-8	Thin brown–greenish deposit layer, mainly due to algal activity and sediment accumulation. Variable thickness ~ 1–2 mm.	mortar
8	CN-9	Thin layer of inconsistent whitish deposit alternating with reddish areas. Presence of encrusting algae and sediment accumulation. Variable thickness ~ 1–2 mm.	mortar
9	CN-10	Thin layer of compact and coherent whitish deposit, alternating with reddish brown areas. Presence of encrusting algae in addition to green and brown algae. Variable thickness ~ 1–8 mm.	mortar
10	CN-12	Layer of whitish deposit, alternating with green and brown areas. Recognized organisms: benthic communities as tube-building annelid worms (Serpulidae) and encrusting algae. There are also green and brown algae. Variable thickness up to several cm.	mortar
11	CN-13	Thin layer of reddish-brown deposit. Poor presence of benthic communities in which encrusting algae prevail in addition to green and brown algae. Variable thickness ~ 1–4 mm.	mortar
12	CN-14	Compact and coherent layer of whitish color, alternating with red–brown areas. Presence of encrusting algae, red, green and brown algae. Variable thickness up to several cm.	mortar
13	CN-15	Compact and coherent layer of whitish color, alternating with red–brown areas. Presence of encrusting algae, red, green and brown algae. Variable thickness up to several cm.	mortar
14	CN-16	Slight reddish-brown deposit layer. Poor presence of benthic communities in which green and brown algae prevail. Variable thickness ~ 1–2 mm.	mortar
15	CN-17	Compact and coherent deposit layer of brownish-green color, alternating with reddish areas. Presence of encrusting algae, green and brown algae. Variable thickness up to several cm.	mortar
16	CN-18	Compact and coherent layer of whitish color, alternating with red–brown areas. Presence of encrusting algae and bryozoans. Variable thickness ~ 1–3 mm.	ceramic fragment + mortar
17	CN-19	Compact and coherent deposit layer of reddish color attributable almost exclusively to the presence of encrusting algae. Variable thickness up ~ 2–3 mm.	mortar

Mortar surfaces were colonized by different encrusting organisms including barnacles, tubeworms, bryozoans, mollusks, and coralline algae, with barnacles and tubeworms apparently being the most abundant. Tubeworms were observed randomly distributed on samples (Figure 3A), while barnacles occupied large portions of the sample surfaces and their structures firmly adhered to mortar surfaces (Figure 3B).

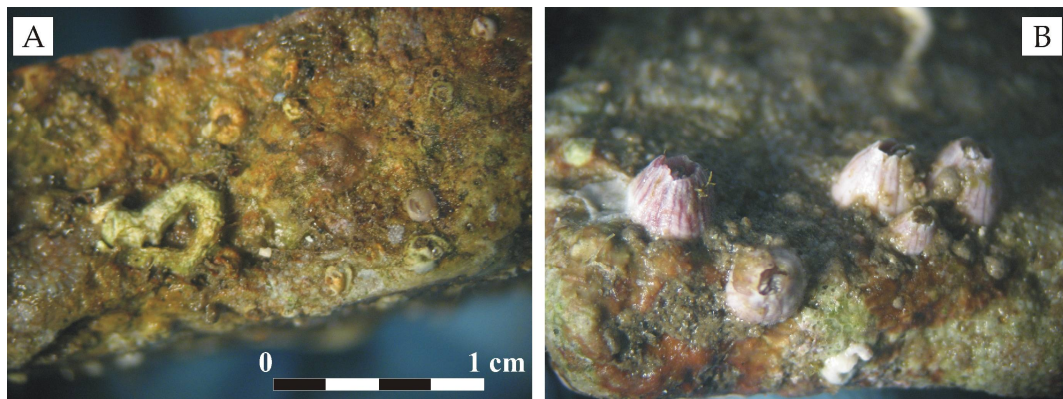


**Figure 3.** Macroscopic view of specimens: tubeworms (A) and barnacles (B) are among the most abundant encrusting organisms in the studied samples.

### 3.2. Thin-Section Petrography by Optical Microscopy (OM)

Thin-section observations by means of an optical microscope on mortar samples led to the identification of the main compositional and textural characteristics of the collected samples. Small differences in term of aggregate/binder ratio, relative abundances of the various aggregate components, and presence of minor constituents were highlighted. On this basis, the recipes of mortars used for building up the fishpond structure in the pilot site were assessed.

The diagnostic features recognized for each sample are schematically summarized in Table 2. Some representative photomicrographs are shown in Figure 4. In particular, mortar samples show as distinctive ‘marker’ the presence of trachyte rocks, pumice, and glassy scoriae fragments (with a variable relative abundance ratio), apparently predominating over all the other constituents. The frequency of the aggregate grains oscillated from a minimum of 10% up to 40%. Samples were characterized by non-homogeneous sorting with a grain size distribution mainly ranging from the fine sand class (0.125–0.25 mm) to very coarse sand (1–2 mm). Granules composed of single volcanic minerals (e.g., alkali feldspar, clinopyroxene, biotite) were always present as common to sporadic components of the aggregate. Ceramic fragments were detected as minor constituents of the aggregate only in samples CN-9, 10, 13, and 15. The majority of the samples had a binder characterized by a clumpy texture without optical activity mixed with smaller patches with weak aggregate birefringence. These non-birefringent portions of the binder could consist of amorphous or weakly crystalline phases formed after ‘pozzolanic’ reactions. In fact, they were highlighted above all on the interfaces between aggregate granules (mainly glassy scoriae and pumices) and binder, while the birefringent portion was constituted by microcrystalline calcite.

Table 2. Mineralogical and textural features of mortar samples.

Sample Code	Aggregate					Binder		
	Prevailing Size (mm)	Packing (%)	Mineralogical Phases	Rock Fragments	Bioclasts/Limestone Fragments	Cocciopesto	Texture	Optical Activity
CN-1	0.5–1	40	Fs (+ +), Qtz (r)	trachyte (+ +), pumice (+), glassy scoriae (r)	-	-	sporadic lumps	inactive
CN-1M	0.5–1	30	Cpx (+ +); Fs (+), Qtz (r); Op (r);	trachyte (+ +), pumice (+), glassy scoriae (r)	+	-	rare lumps	slightly active
CN-2	0.5–1.5	50	Cpx (+ +); Fs (+); Qtz (r)	trachyte (+ +), glassy scoriae (r)	-	-	common lumps	inactive
CN-2M	0.5–2	20–30	Cpx (+ +); Fs (+), Qtz (r)	trachyte (+ +), glassy scoriae (r)	-	-	sporadic lumps	slightly active
CN-4	0.5–1	10	Fs (+ +); Cpx (r), Qtz (r)	pumice (+ +), glassy scoriae (+)	+ +	-	common lumps	slightly active
CN-7	0.5–1.5	15	Fs (+ +); Cpx (+ +); Qtz (r); Bt (r);	trachyte (+ +), pumice (+), glassy scoriae (r)	-	-	common lumps	slightly active
CN-8	0.5–2	10–15	Fs (+ +); Cpx (+ +); Qtz (r); Bt (r)	pumice (+ +), glassy scoriae (+); trachyte (+)	-	-	sporadic lumps	slightly active
CN-9	0.5–2	30	Fs (+ +); Cpx (+ +); Qtz (r); Op (r)	pumice (+ +), glassy scoriae (+); trachyte (+)	+	(r)	common lumps	slightly active
CN-10	0.5–1	35	Fs (+ +); Cpx (+ +); Qtz (r); Pl (r)	glassy scoriae (+); trachyte (+)	-	+	sporadic lumps	slightly active
CN-12	0.5–1.5	30	Fs (+ +); Cpx (+); Qtz (r)	pumice (+ +), glassy scoriae (+)	-	-	common lumps	inactive
CN-13	0.5–1.5	25	Fs (+ +); Cpx (+); Qtz (r)	pumice (+), glassy scoriae (+)	-	+	abundant lumps	slightly active
CN-14	0.5–2	40	Cpx (+ +); Fs (+); Qtz (r); Pl (r); Bt (r); Op (r)	trachyte (+ +), pumice (+), glassy scoriae (+)	-	-	sporadic lumps	inactive
CN-15	0.5–1.5	30	Qtz (r); Bt (r)	pumice (+ +), glassy scoriae (+); trachyte (+)	-	+	common lumps	inactive
CN-16	0.5–1	30	Cpx (+ +); Fs (+); Qtz (r); Pl (r); Bt (r)	trachyte (+ +), pumice (+), glassy scoriae (r)	-	-	sporadic lumps	slightly active
CN-17	0.5–1	10–15	Fs (+ +); Cpx (+); Op (+); Qtz (r)	trachyte (+ +), pumice (+), glassy scoriae (r)	-	-	rare lumps	inactive
CN-18	0.2–0.5	40	Fs (+ +); Cpx (+); Qtz (r)	trachyte (+ +); pumice (+ +), glassy scoriae (+)	-	-	sporadic lumps	inactive
CN-19	0.5–2	40	Fs (+ +); Cpx (+); Qtz (r)	trachyte (+); pumice (+); glassy scoriae (+)	-	-	sporadic lumps	slightly active

Legend: Pl = plagioclase; Fs = feldspar; Cpx = clinopyroxene; Qtz = Quartz; Bt = Biotite; Op = opaque mineral; + + = abundant, + = common, + = sporadic/rare; - not detected.

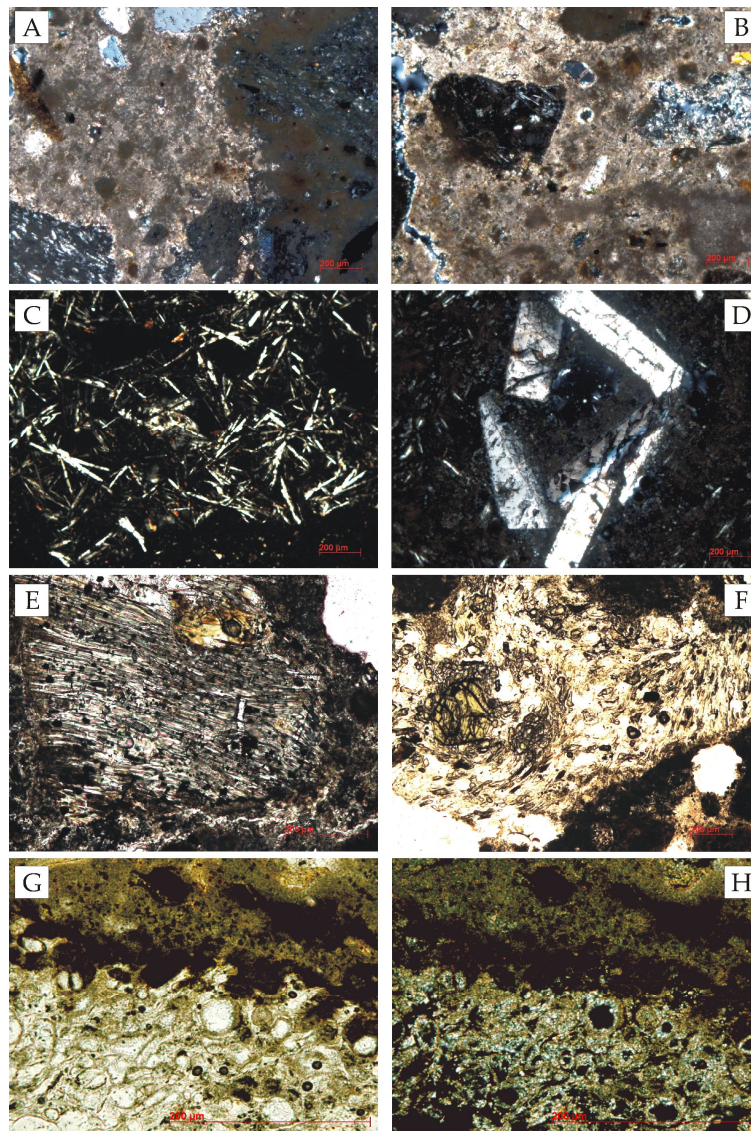


**Figure 4.** Some of the representative mortars: (A,B) cryptocrystalline and recrystallized aspect of the binder and aggregate constituted by trachytic rock fragments and glassy scoriae; (C) minute tabular crystals of sanidine in a trachytic fragment; (D) detail of tabular crystals of sanidine; (E,F) glassy scoriae and pumice fragments constituting the aggregate (clinopyroxene crystals are also evident); (G,H) non-birefringent portions of the binder at the interfaces with pumices fragment.

Besides, several lime lumps were also recognized from rare to common constituents. They often appeared fractured, scarcely compact with not well-defined edges.

### 3.3. X-ray Powder Diffraction Analysis (XRPD)

This section discusses the results obtained from the interpretation of the XRPD patterns for three representative mortars. The XRPD patterns showed that despite the separation of the binder from the aggregate granules, some recognized mineralogical phases belonged to the aggregate sand, while the binder was composed of calcite (Figure 5). Therefore, pyroxene, feldspars (sanidine and plagioclase), hematite, and small amounts of quartz were part of the sandy aggregate added to a lime-based binder.

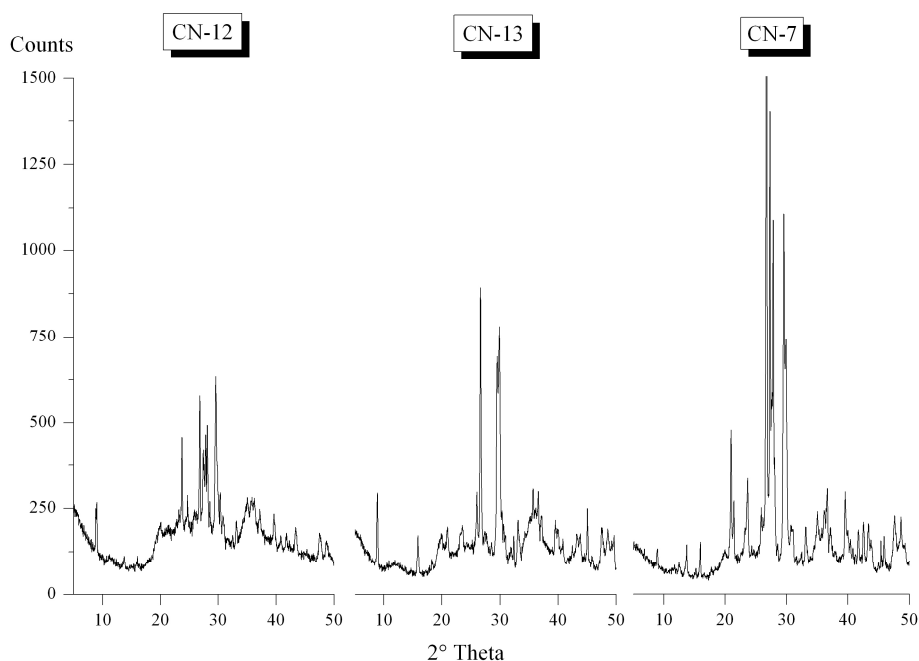


**Figure 5.** XRPD patterns of the three representative samples of mortars.

It is also possible to notice that the calcite appeared to be relatively more abundant (effect  $d_{104}$  more intense) in the binder of the sample CN-7 compared to the samples CN-12 and CN-13. The above-mentioned phases could obviously be assigned to the presence of small quantities of the finest component of the aggregate belonging to the coarse silt class (0.02–0.06 mm). The relatively lower abundance of calcite found in samples CN-12 and CN-13 can be likely explained by the presence in these samples of a certain percentage of amorphous portion consisting of calcium hydrate silicate (CSH) and calcium hydrate aluminate (CAH). The expected main XRD peaks of CSH were not observed in the carbonated lime. This was probably due to the amorphous character of CSH (low-crystallinity phases with different structures) or its principal peaks overlap with calcite. The fact that the peaks for CSH phases were not measured in mortar samples does not mean that they were not present, but rather, they may exist in the form of gels of very low crystallinity [17]. This result, according to the previously described petrographic data, was due to the occurrence of pozzolanic reactions that significantly compose large portions of the background matrix (binder) characterized by optical inactivity. In fact, as already reported in previous studies [18,19], the volcanic rock fragments composing the aggregates could cause the hydraulicization of the binder and the formation of these new phases, whose presence is demonstrated by observing, through optical microscopy, the reaction rims around the fragments of the aggregate.

To be noted also was the presence of a clay component attributable to the reaction between seawater (strongly concentrated in some alkaline ions) with a pre-existing mineralogical phase composing the aggregate.

Finally, the presence of Kieserite ( $MgSO_4 \cdot H_2O$ ), magnesium sulphate, as a mineralogical phase of neoformation, despite the prewashing procedure carried out before proceeding to the preparation of the powders, was highlighted. This mineral was found in particular in greater quantities in the sample CN-13.

#### 3.4. Electron Probe Micro Analysis Equipped with Energy-Dispersive Spectroscopy (EPMA-EDS)

Table 3 reports the mean values of the major elements detected after 10 measurements performed for each investigated mortar sample. All the samples showed a high amount of CaO ranging from a minimum value of 69.1 wt% for sample CN-13 to a maximum of 86.3 wt% for CN-17. Furthermore, the

content in SiO<sub>2</sub> was not negligible, varying from 0.41 wt% for CN-7 to 12.13 wt% for CN-12. These data were useful to evaluate the hydraulic index according to [16], also considering the amount of Al<sub>2</sub>O<sub>3</sub>, Fe<sub>2</sub>O<sub>3</sub>, and MgO. By observing the data in Table 3, it is evident that the HI showed values greater than 0.1 for most of the samples, thus indicating evident phenomena of hydraulicization of the binder [17]. In particular, the hydraulicity index showed values ranging between 0.02 and 0.23, with samples CN-2M, CN-4, CN-7, and CN-9 falling in the field of aerial lime (HI < 0.10), samples CN-1, CN-1M, CN-2, CN-8, CN-10, CN-17, and CN-18 falling within the field of weakly hydraulic limes (0.10 < HI < 0.16), and samples CN-12, CN-13, CN-14, CN-15, and CN-19 in the range of moderately hydraulic limes (0.2 < HI < 0.4).

**Table 3.** Average values of major oxides (wt%) determined through electron probe micro analysis energy-dispersive spectroscopy (EMPA-EDS) analysis of binder and lumps.

Sample Code	CaO	Na <sub>2</sub> O	MgO	Al <sub>2</sub> O <sub>3</sub>	SiO <sub>2</sub>	SO <sub>3</sub>	ClO	FeO	SiO <sub>2</sub> + Al <sub>2</sub> O <sub>3</sub> + FeO	CaO + MgO	HI	Type
CN-1	80.71	0.97	3.10	6.78	3.00	0.72	2.17	2.54	12.32	83.82	0.15	WH
CN-1M	84.08	0.38	4.61	1.02	7.60	0.38	0.28	1.63	10.26	88.70	0.12	WH
CN-2	80.94	1.93	5.61	4.48	3.10	0.22	0.95	2.76	10.34	86.55	0.12	WH
CN-2M	82.52	0.75	7.71	4.33	3.92	0.24	0.52	-	8.25	90.23	0.09	A
CN-4	85.25	0.72	12.03	-	0.46	-	-	1.54	2.00	97.28	0.02	A
CN-7	83.99	0.74	12.59	0.98	0.40	-	-	1.30	2.68	96.57	0.03	A
CN-8	77.63	0.58	7.97	4.48	5.92	-	0.89	2.52	12.92	85.60	0.15	WH
CN-9	82.86	-	12.06	0.58	1.49	0.42	-	2.59	4.67	94.92	0.05	A
CN-10	76.14	1.22	5.85	6.40	3.72	1.06	3.14	2.45	12.58	82.00	0.15	WH
CN-12	72.62	-	8.09	2.96	12.13	0.44	-	3.75	18.85	80.71	0.23	MH
CN-13	69.09	0.30	12.48	5.68	8.50	-	-	3.96	18.13	81.57	0.22	MH
CN-14	74.81	0.80	9.05	2.96	8.22	0.59	0.88	2.70	13.88	83.86	0.17	MH
CN-15	73.05	-	10.69	2.86	9.27	0.41	1.24	2.48	14.61	83.74	0.17	MH
CN-16	82.60	0.56	4.98	1.99	4.72	0.50	0.50	4.15	10.86	87.59	0.12	WH
CN-17	86.25	-	2.92	1.72	6.29	-	-	2.82	10.82	89.18	0.12	WH
CN-18	72.81	1.07	8.01	6.42	3.59	0.35	3.62	4.12	14.14	80.82	0.17	WH
CN-19	74.20	-	6.80	5.41	7.14	-	3.50	2.95	15.51	81.00	0.19	MH
Lumps	CaO	Na <sub>2</sub> O	MgO	Al <sub>2</sub> O <sub>3</sub>	SiO <sub>2</sub>	SO <sub>3</sub>	ClO	FeO	SiO <sub>2</sub> + Al <sub>2</sub> O <sub>3</sub> + FeO	CaO + MgO	HI	Type
CN-1	90.96	0.15	1.96	0.67	3.38	0.40	0.26	2.21	6.27	92.92	0.07	A
CN-2	88.47	0.49	3.02	1.13	1.93	0.49	0.19	4.28	7.34	91.49	0.08	A
CN-2M	89.70	0.71	4.11	-	-	0.30	0.54	4.64	4.64	93.81	0.05	A
CN-4	93.82	1.42	-	-	0.70	1.24	-	2.82	3.52	93.82	0.04	A
CN-7	90.59	1.74	0.49	0.54	2.95	1.17	-	2.52	6.01	91.07	0.07	A
CN-8	91.81	1.57	0.48	0.53	1.82	1.20	-	2.58	4.93	92.30	0.05	A
CN-9	90.19	0.44	3.66	1.11	2.35	0.65	-	1.59	5.06	93.85	0.05	A
CN-10	86.25	-	2.92	1.72	6.29	-	-	2.82	10.82	89.18	0.12	WH
CN-12	84.46	-	5.06	2.21	2.97	1.20	2.43	2.69	7.86	89.51	0.09	A
CN-13	80.90	0.95	7.53	3.79	3.32	0.60	1.50	1.41	8.51	88.43	0.10	A
CN-15	82.58	0.39	5.05	3.32	3.08	0.57	1.45	2.56	8.96	87.63	0.10	WH
CN-18	81.40	0.20	3.38	4.02	7.49	0.29	1.04	2.17	13.68	84.78	0.16	WH
CN-19	84.24	0.25	2.32	4.22	4.27	0.18	0.54	3.98	12.47	86.56	0.14	WH

Legend: HI = hydraulicity index; A = aerial lime; WH = weakly hydraulic lime; MH = moderately hydraulic lime; - = not detected.

Moreover, five measurements were performed for detected lumps in the mortars. Lime lumps are usually considered portions of binder not well mixed and/or partially burned limestone residue from the firing process [20,21]. Then, the evaluation of their chemical compositions and HI index allowed for the definition of the aerial and/or hydraulic nature of the binder. The HI related to lumps of samples CN-1, CN-2, CN-2M, CN-4, CN-7, CN-8, CN-9, CN-10, CN-12, and CN-13 showed values from 0.03 to 0.10, as a result of lumps with aerial properties (HI < 0.10), while samples CN-10, CN-12, CN-13, CN-15, CN-18, and CN-19 showed weakly hydraulic properties. These properties might have originated from pozzolanic additives (natural pozzolana) and/or ceramic fragments that reacted with a more or less pure lime binder. These mortars can be thus considered of hydraulic type after the addition of natural volcanic material and cocciopesto, as confirmed by EMPA-EDS results on the binder.

Figure 6 shows the EMPA-EDS image displaying some morphological features and investigated areas within the sample CN-10.

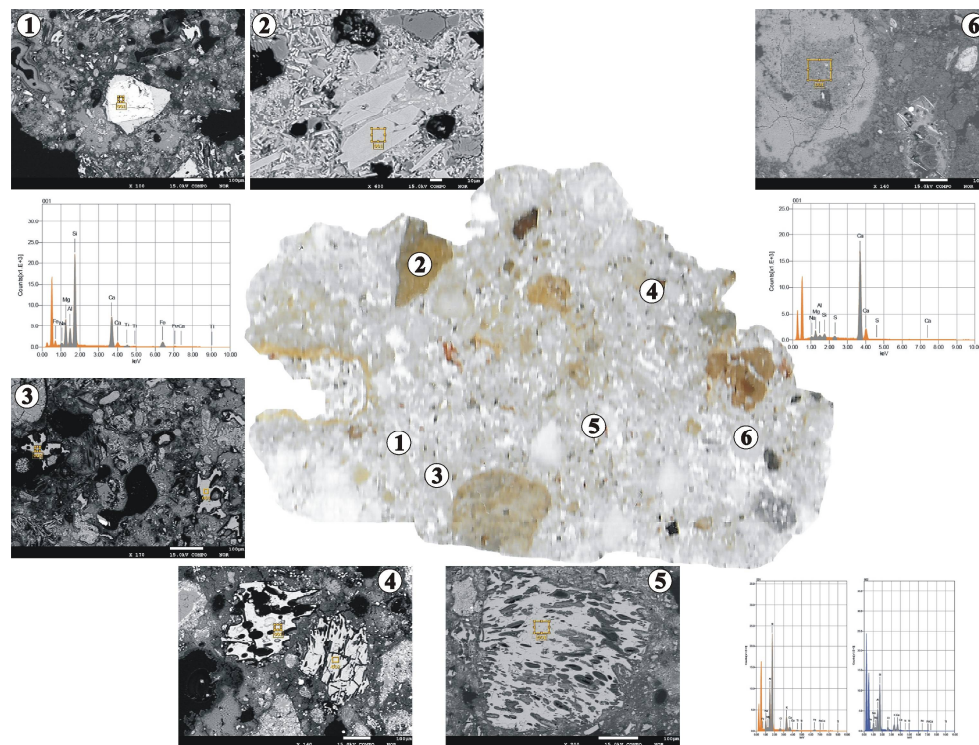


**Figure 6.** Representative EMPA-EDS images showing some morphological features and investigated areas within CN-10 sample: 1 and 2, clinopyroxene crystals and corresponding EDS spectrum; 3, 4, and 5, glassy scoriae, pumice fragments, and corresponding EDS spectra; 6, analyzed lime lump.

Among the investigated area there were also selected glass shards of pumices/glassy scoriae and volcanic minerals (pyroxenes), composing the aggregate of mortar samples.

Chemical analyses of mayor oxides of pumices/glassy scoriae were reported in the TAS diagram (Figure 7A, after [22]), while pyroxene compositions were projected onto the Enstatite–Ferrosilite–Diopside–Hedenbergite Quadrilateral (Figure 7B, after [23]). Pumices/glassy scoriae compositions are sufficiently homogeneous; in fact, most of the samples are concentrated in the class of phonolites and trachytes, showing an evident enrichment in alkalis with relatively constant levels in  $\text{SiO}_2$ . Instead, according to the proposed classification from [23], the composition of the pyroxenes composing the aggregate in the studied mortars fell in the field of diopside. This result would seem to agree with the chemical compositions of the clinopyroxene present in the Roman Magmatic Province reported by various authors [24–30].

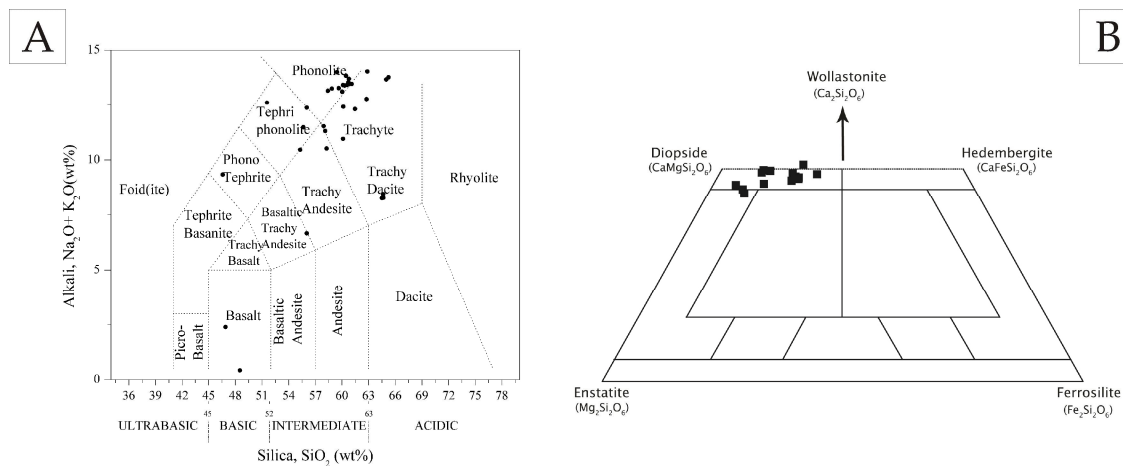


**Figure 7.** (A) Plot of scoriae/pumice composition into the total alkali silica (TAS) diagram [22]; (B) Plot of Cpx composition into the classification diagram for Ca–Mg–Fe pyroxenes [23].

#### 4. Conclusions

This archaeometric study provided interesting information both on the mortars used in the archaeological site of Santa Marinella and on their production technology.

In particular, the data obtained allowed us to define the main constituents of historic mortars, but at the same, it was possible to identify the various degradation processes that are of concern. The raw materials used, in fact, were fairly homogeneous, both in term of compositional and textural features, thus confirming the typical "recipe" used in Roman times to realize hydraulic mortars by adding natural pozzolana. Trachyte, pumice, and glassy scoriae fragments are the main constituents composing the sandy aggregate. Monomineralic grains of alkali feldspar, clinopyroxene, and biotite are also present. Chemical compositions (major oxides) of pumice and glassy scoriae fragments as well as of clinopyroxenes are compatible with volcanic products pertaining to the Roman Magmatic Province. It is worth emphasizing that for the attribution of the components constituting the aggregate to the various Italian magmatic provinces, further investigations will be necessary, in particular chemical analyses of the minor and trace elements, as renowned chemical markers of specific magmatic products.

With regard to the binder composition, the analyzed mortars can be all classified as lime mortar with hydraulic character obtained by mixing lime with natural pozzolana and/or by mixing lime with man-made materials (cocciopesto).

The presence of many lumps in the majority of the samples are most likely due to an incomplete mixing of lime and aggregate. In addition, technologies based on the non-seasoning of lime, which produces mixtures with low plasticity, could probably be used [31].

The obtained data concerning the textural, mineralogical, and geochemical information represent the first step both for the formulation of restoration mortars and for the definition of programmed maintenance protocols. Given the importance of the site, this dataset will be used for the development of new restoration mortars that will be applied and tested in situ to consolidate the wall structures. Regarding the biological issue, novel antifouling agents will be formulated, tested, and added to restoration mortar with the aim to slowdown of biological colonization.

**Author Contributions:** L.R. participated in the fieldwork, the elaboration of laboratory tests, the interpretation of the results, and wrote the manuscript. M.R. participated in the fieldwork, the elaboration of laboratory tests, and contributed to the manuscript writing. S.R. participated in the elaboration of laboratory tests and contributed to the manuscript writing. M.A. participated in the fieldwork. F.E. and B.D.P. assisted in the fieldwork. M.F.L.R. participated in writing—review of the manuscript, project administration, and funding acquisition.

**Funding:** "MaTACoS—Materiali e Tecnologie avanzate alla Conservazione Subacquea", PON Innovazione e Competitività 2014/2020 MiSE Horizon 2020, Ministero dello Sviluppo Economico "Horizon 2020" PON I&C 2014-2020 FERS AVVISO D.M. del 1 giugno 2016 ASSE I. Prog. n. F/050146/03/X32, CUP: B28I17000360008 COR: 233250.

**Conflicts of Interest:** The authors declare no conflict of interest. The funders had no role in the design of the study; in the collection, analyses, or interpretation of data; in the writing of the manuscript; or in the decision to publish the results.

## References

1. Ricci, S.; Davidde, B.; Bartolini, M.; Priori, G.F. Bioerosion of lapideous artefacts found in the underwater archaeological site of Baia (Naples). *Archaeol. Marit. Mediterr. Int. J. Underw. Archaeol.* **2009**, *6*, 167–186.
2. La Russa, M.F.; Ruffolo, S.A.; Ricci, S.; Davidde, B.; Barca, D.; Ricca, M.; Capristo, V. A Multidisciplinary approach for the study of underwater artefacts: The case of TritoneBarbato marble statue (GrottaAzzurra, Island of Capri, Naples). *Period. Miner.* **2013**, *82*, 101–111.
3. La Russa, M.F.; Ricca, M.; Belfiore, C.M.; Ruffolo, S.A.; ÁlvarezBallester De Buergo, M.; Crisci, G.M. The contribution of earth sciences to the preservation of underwater archaeological stone materials: An analytical approach. *Int. J. Conserv. Sci.* **2015**, *6*, 335–348.
4. La Russa, M.F.; Ruffolo, S.A.; Ricca, M.; Rovella, N.; Comite, V.; De Buergo, M.A.; Barca, D.; Crisci, G.M. Archaeometric approach for the study of mortars from the underwater archaeological site of Baia (Naples) Italy: Preliminary results. *Period Miner.* **2015**, *84*, 1–16.
5. Crisci, G.M.; La Russa, M.F.; Macchione, M.; Malagodi, M.; Palermo, A.M.; Ruffolo, S.A. Study of archaeological underwater finds: Deterioration and conservation. *Appl. Phys. A* **2010**, *100*, 855–863. [[CrossRef](#)]
6. Davidde, B.; Ricci, S.; Poggi, D.; Bartolini, M. Marine bioerosion of stone artefacts preserved in the Museo Archeologico dei Campi Flegrei in the Castle of Baia (Naples). *Archaeol. Marit. Mediterr.* **2010**, *7*, 1000–1041.
7. Bruno, F.; Muzzupappa, M.; Barbieri, L.; Gallo, A.; Ritacco, G.; Lagudi, A.; La Russa, M.F.; Ruffolo, S.A.; Crisci, G.M.; Ricca, M.; et al. The CoMAS project: New materials and tools for improving the in situ documentation, restoration, and conservation of underwater archaeological remains. *Mar. Technol. Soc. J.* **2016**, *50*, 108–118. [[CrossRef](#)]
8. Jackson, M.D.; Deocampo, D.; Marra, F.; Scheetz, B. Mid-Pleistocene pozzolanic volcanic ash in ancient Roman concretes. *Geoarchaeology* **2010**, *25*, 36–74. [[CrossRef](#)]
9. Marra, F.; Anzidei, M.; Benini, A.; D’Ambrosio, E.; Gaeta, M.; Ventura, G.; Cavallo, A. Petro-chemical features and source areas of volcanic aggregates used in ancient Roman maritime concretes. *J. Volcanol. Geotherm. Res.* **2016**, *328*, 59–69. [[CrossRef](#)]
10. Cámara, B.; Álvarez de Buergo, M.; Bethencourt, M.; Fernández-Montblanc, T.; La Russa, M.F.; Ricca, M.; Fort, R. Biodeterioration of marble in an underwater environment. *Sci. Total Environ.* **2017**, *609*, 109–122. [[CrossRef](#)]
11. Enei, F.; Haack, M.L.; Nardi-Combescure, S.; Poccardi, G. *Castrum Novum. Storia e archeologia di una colonia romana nel territorio di Santa Marinella*; Quaderno 1: Santa Marinella, Italy, 2011.
12. Desibio, L.; Enei, F.; Nardi-Combescure, S.; Poccardi, G.; Sia, V.; Levanto, M.T.; Squaglia, A. The CastrumNovum Project: History and Archaeology of a Roman Colony (Santa Marinella, Rome, Italy). *Int. J. Archaeol. Archaeol. Sci.* **2015**, *3*, 62–75. [[CrossRef](#)]
13. Paterakis, A.B. The deterioration of ceramics by soluble salts and methods for monitoring their removal. In *Recent Advances in the Conservation and Analysis of Artefacts*, Institute of Archaeology; Black, J., Ed.; Summer Schools Press: London, UK, 1987; pp. 67–73.
14. Montana, G.; Randazzo, L.; Castiglia, A.; La Russa, M.F.; La Rocca, R.; Bellomo, S. Different methods for soluble salt removal tested on Late-Roman cooking ware from a submarine excavation at the Island of Pantelleria (Sicily, Italy). *J. Cult. Herit.* **2014**, *15*, 403–413. [[CrossRef](#)]
15. Matthew, A.J. Spots before the eyes: New comparison charts for visual percentage estimation in archaeological material. In *Recent Developments in Ceramic Petrology*; Middleton, A., Freestone, I., Eds.; British Museum Occasional Paper: London, UK, 1991; Volume 81, pp. 399–409.
16. Boynton, R. *Chemistry and Technology of Lime and Limestone*, 2nd ed.; Wiley: New York, NY, USA, 1980.
17. Miriello, D.; Barca, D.; Bloise, A.; Ciarallo, A.; Crisci, G.M.; De Rose, T.; Gattuso, C.; Gazineo, F.; La Russa, M.F. Characterisation of archaeological mortars from Pompeii (Campania, Italy) and identification of construction phases by compositional data analysis. *J. Archaeol. Sci.* **2010**, *37*, 2207–2223. [[CrossRef](#)]
18. Taylor, H.F.W. *Cement Chemistry*, 2nd ed.; Thomas Telford Publishing: London, UK, 1997.

19. Hodgkinson, E.S.; Hughes, C.R. The mineralogy and geochemistry of cement/rock reactions: High-resolution studies of experimental and analogue materials. In *Chemical Containment of Waste in the Geosphere*; Metcalfe, R., Rochelle, C.A., Eds.; Geological Society, London, Special Publications: London, UK, 1999.
20. Elsen, J. Microscopy of historic mortars—A review. *Cem. Concr. Res.* **2006**, *36*, 1416–1424. [[CrossRef](#)]
21. Pecchioni, E.; Fratini, F.; Cantisani, E. *Atlante delle Malte Antiche in Sezione Sottile al Microscopio Ottico—Atlas of the Ancient Mortars in thin Section under Optical Microscope*; Nardini Editore: Florence, Italy, 2014.
22. Le Maitre, R.; Streckeisen, A.; Zanettin, B.; Le Bas, M.; Bonin, B.; Bateman, P. (Eds.) *Igneous Rocks: A Classification and Glossary of Terms: Recommendations of the International Union of Geological Sciences Subcommission on the Systematics of Igneous Rocks*; Cambridge University Press: Cambridge, UK, 2002. [[CrossRef](#)]
23. Morimoto, N.; Fabries, J.; Ferguson, A.K.; Ginzburg, I.V.; Ross, M.; Seifert, F.A.; Zussman, J.; Aoki, K.; Gottardi, G. Nomenclature of pyroxenes. *Am. Miner.* **1988**, *73*, 1123–1133.
24. Dallai, L.; Freda, C.; Gaeta, M. Oxygen isotopic geochemistry of pyroclastic clinopyroxene monitors carbonate contributions to Roman-type ultrapotassic magmas. *Contrib. Miner. Petrol.* **2004**, *148*, 247–263. [[CrossRef](#)]
25. Perini, G.; Francalanci, L.; Davidson, J.P.; Conticelli, S. The petrogenesis of Vico Volcano, Central Italy: An example of low scale mantle heterogeneity. *J. Petrol.* **2004**, *45*, 139–182. [[CrossRef](#)]
26. Gaeta, M.; Freda, C.; Christensen, J.N.; Dallai, L.; Marra, F.; Karner, D.B.; Scarlato, P. Time-dependent geochemistry of clinopyroxene from the Alban Hills (Central Italy): Clues to the source and evolution of ultrapotassic magmas. *Lithos* **2006**, *86*, 330–346. [[CrossRef](#)]
27. Boari, E.; Avanzinelli, R.; Melluso, L.; Giordano, G.; Mattei, M.; De Benedetti, A.; Morra, V.; Conticelli, S. Isotope geochemistry (Sr–Nd–Pb) and petrogenesis of leucite-bearing volcanic rocks from “ColliAlbani” volcano, Roman Magmatic Province, Central Italy: Inferences on volcano evolution and magma genesis. *Bull. Volcanol.* **2009**, *71*, 977–1005. [[CrossRef](#)]
28. Marra, F.; Deocampo, D.; Jackson, M.D.; Ventura, G. The Alban Hills and Monti Sabatini volcanic products used in ancient Roman masonry (Italy): An integrated stratigraphic, archaeological, environmental and geochemical approach. *Earth Sci. Rev.* **2011**, *108*, 115–136. [[CrossRef](#)]
29. Belfiore, C.M.; Fichera, G.V.; La Russa, M.F.; Pezzino, A.; Ruffolo, S.A.; Galli, G.D. A Multidisciplinary Approach for the Archaeometric Study of Pozzolanic Aggregate in Roman Mortars: The Case of Villa dei Quintili (Rome, Italy). *Archeometry* **2015**, *57*, 269–296. [[CrossRef](#)]
30. Belfiore, C.M.; Fichera, G.V.; Ortolano, G.; Pezzino, A.; Visalli, R.; Zappalà, L. Image processing of the pozzolanic reactions in Roman mortars via X-ray Map Analyser. *Microchem. J.* **2016**, *125*, 242–253. [[CrossRef](#)]
31. Bakolas, A.; Biscontin, G.; Moropoulou, A.; Zendri, E. Characterization of the lumps in the mortars of historic masonry. *Thermochim. Acta* **1995**, *269–270*, 809–816. [[CrossRef](#)]

